INVESTIGATION OF MACH NUMBER EFFECTS ON AERODYNAMIC NOISE RADIATION BY SUBSONIC JETS

Carlos Anissem Moser, carlos.moser@yahoo.com.br
Marcello Augusto Faraco, marcello@sc.usp.br
Universidade de São Paulo, Department of Aeronautical Engineering

Jorge Hugo Silvestrini, jorgehs@pucr.br
Pontifícia Universidade Católica do Rio Grande do Sul, Department of Mechanical and Mechatronics Engineering

Abstract. *The aerodynamic noise radiation was investigated by the analysis of sound generation and propagation on subsonic jets at high Reynolds number. For the unsteady flow-noise computations, a non-conservative characteristic-based formulation was used to solve by implicit large-eddy simulation (LES) the fully compressible Navier-Stokes equations. The wave modal structure of the flow equations provided by the characteristic-based formulation allows to define non-reflecting boundary conditions and buffer zone treatments especially adapted for aeroacoustic computations. Results for a number of canonical flow configurations have demonstrated the excellent performance of the implicit LES in capturing transition and turbulence decay's in terms of the evolution of kinetic energy dissipation, energy spectra and enstrophy. The direct assessment of sound provided by implicit LES allows to compute jet noise radiation at high Reynolds number, without any subgrid-scale modeling assumption commonly required by traditional LES methods based on acoustic analogies. LES approaches for compressible flows have ranged from the inherently limited Smagorinsky eddy-viscosity type models to more sophisticated dynamic models. Despite the increasing interest in LES methods for sound predictions, not enough attention has been paid to the accuracy of these methods and, in particular, the effects of subgrid-scale modeling. In order to provide highly accurate computations of the nonlinear mechanisms of jet noise generation, the numerical algorithm employed in the present computations was based on high-order compact finite difference schemes for spatial discretisation and a standard fourth-order Runge-Kutta method for time advancement. Numerical instabilities arising from the high-frequency content of the smallest unresolved subgrid scales were removed by the application of optimized high-order compact filters, which provide dissipation at the higher modified wave numbers only, where the spatial discretisation schemes adopted already exhibit significant dispersion errors. Numerical simulations of Mach* 0.9 *cold jets at Reynolds number* 6.5×10^4 *were carried out in order to analyse Mach number effects on sound propagation, as for example, the spatial non-compactness of the sound sources and the highly directional pattern of noise radiation at small angles, which has been observed in experiments and numerical studies with unsteady shear layer flows. The impact of jet inflow conditions was evaluated, particularly the spatial structure of the inflow disturbances on the development of the jet flow and the radiated sound predicted by compressible LES. The present results obtained by the implicit LES procedure were compared with available experimental and numerical results at similar flow conditions taken from the literature.*
Keywords: *Computational Aeroacoustics, Aerodynamic Noise Radiation, Subsonic jets, Mach number effects.*

1. INTRODUCTION

In computational aeroacoustics, the aerodynamic noise was firstly reported by Colonius et al. [1997] who investigated the sound radiated by the vortex pairing process in a two-dimensional mixing layer. The periodic character of this flow, with less extensive unsteady hydrodynamics than jets, facilitates a detailed analysis of the mechanisms of sound generation. Mitchell et al. [1999a] performed direct numerical simulation (DNS) for both the flow and the sound radiated from subsonic and supersonic two-dimensional, axisymmetric jets. The predicted sound was found to agree with predictions of Lighthill's acoustic analogy. Freund et al. [2000] reported the DNS of a turbulent jet at Mach number 1.92. As the flow was nearly isothermal, the principal noise radiation was Mach waves generated by supersonically advecting flow structures. Bogey et al. [2003a] computed by large-eddy simulation (LES) the sound field of a Mach 0.9 jet at a Reynolds number of 6.5×10^4 with the Smagorinsky model. Based on the unsteady flow results obtained, they directly compute the aerodynamic noise. The mean flow and turbulence intensities, as well as sound directivity and sound levels, were found to be in good agreement with experimental data. Bodony and Lele [2005] conducted a systematic investigation of LES's predictive capability for jet noise at the Reynolds number range from 1.3×10^4 to 3.36×10^5. Noise predictions for the unheated and heated jets were in agreement with experimental data [Tanna, 1977], although some discrepancies were observed depending on the jet operating conditions. Bogey and Bailly [2006] showed that inflow conditions, particularly the spatial structure of inflow disturbances, can significantly impact the development of jet flows and the radiated sound predicted by compressible LES at high Reynolds numbers. Some attempts for round jets have been made by Choi et al. [1999] and Boersma and Lele [1999]. Nevertheless, except for some studies of Bogey and Bailly [2002c, 2003b,c, 2006] and Bodony and Lele [2005], the highest Reynolds numbers reached in the LES simulations are still far bellow those of practical interest. Thus, high Reynolds number calculations of compressible free shear layer flows would be very helpful for analysing the broad-band noise spectrum and understanding of nonlinear mechanisms of noise generation.

1.1 Large-eddy simulation of compressible flows

In the last few years, the LES method has achieved significant progress due to advances in computational power, numerical algorithms and subgrid-scale models. LES has been applied into a wide variety of turbulent flows, ranging from problems of scientific interest to those with engineering applications. This trend has been motivated by the need to provide a more realistic characterization of complex unsteady flows encountered in areas such as flow control, aeroacoustics and fluid/structure interaction. However, the vast majority of LES research has been devoted to incompressible flows; while compressible flow applications have only recently gained some attention, due to the increased complexity introduced by the need to model the energy equation [Pascarelli et al., 2000, Yan and Knight, 2002]. Early applications of LES to compressible flows have used a transport equation for the internal energy per unit mass [Moin et al., 1991, El-Hady et al., 1994] or for the entalphy per unit mass [Speziale et al., 1988, Erlebacher et al., 1992].

LES methods for compressible flows have ranged from using the inherently limited Smagorinsky eddy-viscosity type models, to more sophisticated and accurate dynamic models. The Smagorinsky-type models exhibit two major drawbacks. They ignore turbulence anisotropy and use a local balance assumption between the subgrid scale turbulence kinetic energy production and its dissipation. Furthermore, they predict non-vanishing subgrid eddy viscosity in regions where the flow is laminar, i.e. the eddy viscosity should be zero. The dynamic procedure [Germano et al., 1991, Lilly, 1992] for computing the model coefficient from the resolved velocity field, which requires no adjustable constant, overcome the shortcoming of the Smagorinsky-type models. However, numerical stabilization procedures become complicated when the dynamic model is applied to flow configurations in which there are inhomogeneous directions. Recently, Vreman [2004] developed a new subgrid eddy-viscosity model especially suitable for laminar shear flows, since it vanishes subgrid dissipation in the laminar region and does not require any averaging or clipping procedure for numerical stabilization. Park et al. [2006] proposed a dynamic procedure for determining the model coefficient utilizing the global equilibrium between the subgrid dissipation and the viscous dissipation. In this approach, the model coefficient is globally constant in space but varies in time, and it still garantees zero eddy viscosity in the laminar flow regions.

In traditional LES solution methods, the equations are obtained by applying a spatial filtering to the flow variables. Ideally, for incompressible flows the filtering of the Navier-Stokes equations generates a closure problem in the form of an unknown residual subgrid-scale stress tensor:

$$\tau_{i,j} = \overline{u_i u}_j - \bar{u}_i \bar{u}_j, \tag{1}$$

It should be emphasized that the subgrid-scale stress tensor stems from a closure problem introduced by the spacial filtering and not from the discretization's inability to represent the small scales in the flow. As a result, the subgrid-scale stress tensor strongly depends on the assumed filter shape, which causes a subgrid-scale model to be inherently filter dependent. Thus, depending on the choice of the filter, the corresponding model should satisfy very different requirements in terms of large scale dynamics and kinetic energy budget.

1.1.1 High-order low-pass spatial filtering

The analysis of the impact of spatial discretization errors on LES establishes the need of high order low-pass spatial filtering techniques [Gaitonde and Visbal, 1999]. The high order filtering of Navier-Stokes equations should provides dissipation at the higher modified wave numbers only, where the spatial discretization already exhibits significant dispersion errors, and enforce numerical stability on nonuniform grids. The filtering also should allow to eliminate numerical instabilities arising from poor grid quality, unresolved scales, or boundary conditions, which left to grow can potentially corrupt the solution. The filtering operation is defined by Leonard [1974] as follows

$$\bar{f}(x) = \int_{\Omega} f(x') G(x, x'; \bar{\Delta}) dx', \tag{2}$$

where Ω is the entire domain, G is the filter kernel function and $\bar{\Delta}$ is the filter width associated to the smallest scale retained by the filtering operation. Thus, $\bar{f}$ defines the size and structure of the small scales. If a typical component of the flow solution vector is denoted by f, filtered values at interior points $\bar{f}$ must satisfy

$$\alpha_f \bar{f}_{i-1} + \bar{f}_i + \alpha_f \bar{f}_{i+1} = \sum_{n=0}^{N} \frac{a_n}{2} (f_{i+n} + f_{i-n}), \tag{3}$$

where the $N+1$ coefficients, $a_0, a_1, ..., a_n$ are derived in terms of α_f with Taylor and Fourier-series analysis [Gaitonde and Visbal, 1998, 1999]. In principle, for proper resolution of low wavenumbers, the filter accuracy should be equal or greater than the corresponding accuracy of the spatial discretization scheme. The dissipation characteristics of the filter as function of the scaled wave number (w) is given by the spectral frequency (SF) response of the filtering operator

$$SF(w) = \frac{\sum_{n=0}^{N} a_n \cos(nw)}{1 + 2\alpha_f \cos(w)}, \tag{4}$$

which has $N+2$ unknowns, consisting of $\alpha_f, a_0, a_1, ..., a_n$. To obtain these coefficients, the highest frequency wave modes are eliminated by enforcing the condition $SF(\pi) = 0.0$. Additionally, the variable α_f is usually retained as a free parameter in order to provide some control on the filtering. Because of the form of the denominator of Eq. (4) and for proper behavior of the spectral frequency (SF) response, α_f must be in the range $-0.5 < \alpha_f < 0.5$, with higher values of α_f corresponding to less dissipative implicit filters. By contrast, the explicit filter ($\alpha_f = 0$) display significant degradation of the spectral frequency response and may introduce artificial dispersion as the order of accuracy of the numerical scheme is reduced. The spectral properties of these filters was extensively examined by Gaitonde et al. [1997].

1.2 Implicit large-eddy simulation

An alternative approach to the subgrid type models is the use of high-order spacial filters to implictly model the energy content present in the poorly resolved smallest scales of the flow, with no additional subgrid scale stress or heat flux terms added to the governing equations because of the model. Although the filter is applied explicitly to the evolving solution, this approach is referred as implicit LES, since the application of the spatial filter is a fundamental component to mantain stability by removing high-frequency spurious numerical oscillations. The basis of the implicit approach is that the numerical truncation error associated with the discretization has similar form or action to the subgrid model. Such implicit approach falls into the class of structural models. As there is no assumed form of the nature of the subgrid flow, the subgrid model is entirely determined by the structure of the resolved flow [Sagaut, 2001]. Nevertheless, even with the recently increase of interest in implicit LES, there is not a consensus on the appropriate form of the discretization error, since it is assumed that the numerics provide sufficient modeling of the subgrid terms to allow correct dissipation of turbulent kinetic energy.

In order to mantain acceptable numerical acurracy and proper resolution of low wavenumbers, the flow solution variables are filtered in every spatial direction at the final stage of each time step of the temporal integration using sixth-order low-pass implicit filters [Visbal and Gaitonde, 2001, Visbal and Rizzetta, 2002] combined with high-order compact finite difference schemes [Lele, 1992] for the spatial discretization.

The implicit filtering approach is described as follows

$$\alpha_f \overline{f}_{i-1} + \overline{f}_i + \alpha_f \overline{f}_{i+1} = \sum_{n=1}^{4} \frac{a_n}{2} \left(f_{i+n-1} + f_{i-n+1} \right) \qquad \forall i = 4, ..., n_x - 3, \tag{5}$$

with

$$a_1 = \tfrac{11}{16} + \tfrac{5}{8}\alpha_f, \qquad a_2 = \tfrac{15}{32} + \tfrac{17}{16}\alpha_f, \qquad a_3 = -\tfrac{3}{16} + \tfrac{3}{8}\alpha_f, \qquad a_4 = \tfrac{1}{32} - \tfrac{1}{16}\alpha_f,$$

where α_f should satisfy the inequality: $-0.5 \leq \alpha_f \leq 0.5$. Filters less dissipative are obtained with higher values of α_f, and for $\alpha_f = 0.5$ there is no filtering effect. A detailed analysis of the spectral response of this filter may be found in Gaitonde et al. [1997] and Gaitonde and Visbal [1998].

As the implicit filter (5) has a right-hand side stencil of seven points, obviously it can not be employed near the boundaries of the computational domain. Thus, the following implicit filter will be used for the neighbor points of the boundary point $i = 1$:

$$\alpha_f \overline{f}_{i-1} + \overline{f}_i + \alpha_f \overline{f}_{i+1} = \sum_{n=1}^{7} a_{n,i} f_n \qquad i = 2, 3. \tag{6}$$

For $i = 2$:

$$a_{1,2} = +\tfrac{1}{64} + \tfrac{31}{32}\alpha_f, \qquad a_{2,2} = +\tfrac{29}{32} + \tfrac{3}{16}\alpha_f, \qquad a_{3,2} = +\tfrac{15}{64} + \tfrac{17}{32}\alpha_f, \qquad a_{4,2} = -\tfrac{5}{16} + \tfrac{5}{8}\alpha_f,$$
$$a_{5,2} = +\tfrac{15}{64} - \tfrac{15}{32}\alpha_f, \qquad a_{6,2} = -\tfrac{3}{32} + \tfrac{3}{16}\alpha_f, \qquad a_{7,2} = +\tfrac{1}{64} - \tfrac{1}{32}\alpha_f.$$

For $i = 3$:

$$a_{1,3} = -\tfrac{1}{64} + \tfrac{1}{32}\alpha_f, \qquad a_{2,3} = +\tfrac{3}{32} + \tfrac{13}{16}\alpha_f, \qquad a_{3,3} = +\tfrac{49}{64} + \tfrac{15}{32}\alpha_f, \qquad a_{4,3} = +\tfrac{5}{16} + \tfrac{3}{8}\alpha_f,$$
$$a_{5,3} = -\tfrac{15}{64} + \tfrac{15}{32}\alpha_f, \qquad a_{6,3} = +\tfrac{3}{32} - \tfrac{3}{16}\alpha_f, \qquad a_{7,3} = -\tfrac{1}{64} + \tfrac{1}{32}\alpha_f.$$

Analogously, at the points near the boundary point N:

$$\alpha_f \overline{f}_{i-1} + \overline{f}_i + \alpha_f \overline{f}_{i+1} = \sum_{n=1}^{7} a_{n,N-i+1} f_{N-n+1} \qquad i = N-2, N-1, \tag{7}$$

while, for the boundary points $i = \{1, N\}$, the flow variables are kept without application of any filtering operation.

2. FLOW CONFIGURATION

2.1 Axisymmetric round jet

In the present work was adopted the hyperbolic tangent velocity profile employed by Bogey et al. [2003a] in the computation by LES of the aeorodynamic noise radiation on axisymmetric round jets. This profile is given as follows

$$u(r) = \frac{U_j}{2}\left(1 + \tanh\left(\frac{\mathrm{r_o} - \mathrm{r}}{2\delta_\theta}\right)\right) \tag{8}$$

where U_j is the jet centerline velocity at the inlet, r_o is the half jet diameter D and δ_θ is the inlet shear layer momentum thickness, with $u(r_o) = U_j/2$. The Reynolds number of the flow based on the jet diameter is

$$Re_D = \frac{U_j \times D}{\nu}, \tag{9}$$

where ν is the dynamic viscosity.

2.2 Near-inflow excitation

In order to quickly startup the turbulent mixing process in the jet shear layer, a periodic excitation is applied to the velocity field in the shear layer, just downstream of the inflow boundary. This control strategy is analogue to that used to control the vortex pairing process in mixing layers [Moser et al., 2006]. With the purpose of minimizing reflections of spurious acoustic waves at the inlet boundary, the excitation needs to be essentially incompressible, i.e. with zero divergence [Bogey and Bailly, 2005a]. The axisymmetric structure of this excitation has the form of an elementary vortex ring of radio r_o with streamwise and transverse velocities described by

$$\begin{cases} U_{x_o} = \quad 2\,\frac{r_o}{\Delta_o}\,\frac{y-y_o}{r}\,\exp\left(-\ln 2\,\frac{(\mathrm{x}-\mathrm{x_o})^2+(\mathrm{y}-\mathrm{r_o})^2}{\Delta_\mathrm{o}^2}\right) \\ \\ U_{y_o} = -2\,\frac{r_o}{\Delta_o}\,\frac{x-x_o}{r}\,\exp\left(-\ln 2\,\frac{(\mathrm{y}-\mathrm{y_o})^2+(\mathrm{y}-\mathrm{r_o})^2}{\Delta_\mathrm{o}^2}\right) \end{cases} \tag{10}$$

where $r = \sqrt{x^2 + y^2}$ and Δ_o is the minimum grid spacing in the shear layer. $x_o = 0.80 r_o$ and $y_o = 0$. The aerodynamic fluctuations of velocity given by Eqs.(10) are added to the velocity field at each time step t as follows

$$\begin{cases} u_x = u_x + U_{x_o} U_j \sum_{n=0}^{1} \alpha_n \cos(2\pi f_n t + \phi_n) \\ \\ u_y = u_y + U_{y_o} U_j \sum_{n=0}^{1} \alpha_n \cos(2\pi f_n t + \phi_n) \end{cases} \tag{11}$$

where α_n and ϕ_n are the amplitudes and phases corresponding to each one of the frequencies of excitation f_n. The characteristic velocity scale on the jet shear layer is the ambient sound speed c_o. The development of aerodynamic fluctuactions of velocity on the jet shear layer is governed by two different modes, which are associated with two different characteristic length scales. These length scales are the shear layer momentum thickness δ_θ and the jet diameter D. The first mode is the fundamental frequency f_o, which is observed in the neighborhood of the jet inlet. This mode is responsible by the exponential growth of the shear layer instabilities. For the hyperbolic tangent velocity profile (8), the linear instability theory [Michalke, 1964] predicts that the strongest amplification rate of perturbations is observed for

$$f_o = 0.017 \frac{U_j}{\delta_\theta}. \tag{12}$$

The second mode, known as the first sub-harmonic $f_1 = f_o/2$, corresponds to the frequency of the velocity fluctuations that occurs in the jet potential core. This mode is characterized by the Strouhal number

$$St = \frac{f \times D}{U_j}, \tag{13}$$

which was observed experimentally [Juvé et al., 1980, Stromberg et al., 1980] in the range $0.2 < St < 0.5$.

3. NUMERICAL RESULTS

In the present study, the jet Reynolds number was chosen as $Re_D = 6.5 \times 10^4$ and the Mach number was set to $M = 0.9$, which leads to the jet centerline velocity $U_j = 0.9 c_o$. The choice of the jet Mach number 0.9 may be justified by the considerable amount of numerical and experimental studies available in the literature for subsonic jets at high Mach numbers [Bogey et al., 2003a, Lau et al., 1993, Lush, 1971, Mollo-Christensen et al., 1964, Stromberg et al., 1980].

This Reynolds number also corresponds to an intermediate value between jets obtained by DNS with Re_D of order 10^3 and experimental jets, with $Re_D \geq 10^5$. For $Re_D \geq 10^5$ the number of points necessary for discretization would be exorbitant, since the jet exit shear layer is very thin [Zaman, 1985] with momentum thickness of the order of $10^{-3}D$. The momentum thickness $\delta_\theta = 0.05r_o$ was considered, which affords the development of vortical structures in the shear layer region before occuring the turbulent mixing, i.e. before the end of the jet potential core. The parameters of the exitation for the two frequencies f_o and f_1 were fixed as $\alpha_o = 3.6 \times 10^{-3}$ and $\alpha_1 = \alpha_o/3$ for the amplitudes, and $\phi_o = 0$ and $\phi_1 = \pi/2$ for the phases. Reflections of spurious waves generated by the excitation at the inflow boundary were minimized by applying an acoustic abosorbing zone in the neighborhood of excitation [Moser et al., 2006].

In order to reduce the inherently high computational cost of the three-dimensional aeroacoustic computations, the preliminary tests of validation involving implicit large-eddy simulations of subsonic jets were carried out in a two-dimensional domain with size 50×50, which was discretized in a Cartesian grid with 255×225 points. As shown Figure 1 the mesh is gradually stretched in both directions. As the velocity gradients are more pronounced in the transverse direction, the mesh is more refined in this direction, with a minimum uniform spacing of $\Delta y_{min} = 0.060r_o$ in the jet shear layer region. Out of this region the grid spacing increases exponentially up to a maximum uniform spacing of $\Delta y_{max} = 0.602r_o$ in the region of the acoustic field. In the streamwise direction, as the gradients of velocity are less important than the transverse direction, the spatial discretization is relatively coarser. The mesh has a minimum uniform spacing of $\Delta x_{min} = 0.071r_o$ in the region of jet potential core. Downstream of this region the grid is gradually stretched up to a maximum grid spacing of $\Delta x_{max} = 1.402r_o$ at the outflow boundary.

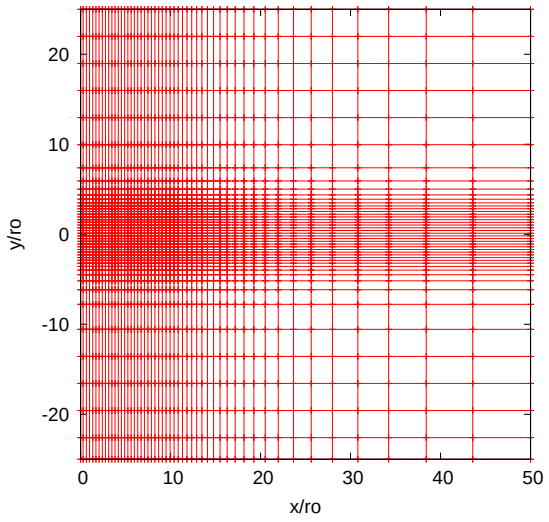

Figure 1. Grid discretization in the computational domain. Representation of one grid point over five in both directions.

3.1 Aerodynamic sound source

The aerodynamic near-field mixing region of the two-dimensional round jet is represented in Fig. 2 by the vorticity $\omega_{xy} = \partial v/\partial x - \partial u/\partial y$. The introduction of a periodic excitation (identified by the two small lobes axisymmetrically

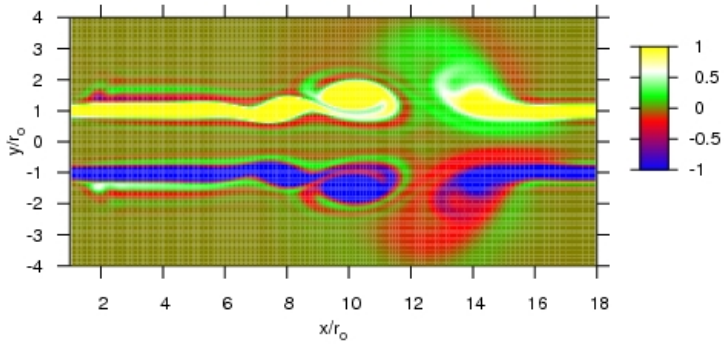

Figure 2. Near-field aerodynamic sound source region of the jet represented by the vorticity field ω_{xy}. Computational domain for $1 < x/r_o < 18$ and $-4 < y/r_o < 4$ with buffer zone of aerodynamic dissipation located after $x = 15r_o$.

distributed near the jet inlet), trigger a growth of the shear layer instabilities, which rapidly evolve downstream to form axisymmetric coherent vortical structures. The approximation and interaction of two consecutive vortical structures in the shear layer give rise to the vortex pairing process, which occurs at a fixed position around $x = 10r_o$ every period of time $T_p = 1/f_p$, with frequence $f_p = f_o/2$, where f_o is the fundamental frequency of the excitation. It should be remarked that vortical structures which are eventually originated after the vortex pairing process must be rapidly dissipated in the buffer zone (located after $x = 15r_o$), in order to avoid the development of other pairings which may introduce undesirable secondary sound sources in the jet shear layer.

A detailed description of the aerodynamic development of the vortex pairing process on the jet shear layer region is depicted in Fig. 3 by the snapshots of the vorticity ω_{xy} at four successive instants of time separated by $T_p/4$. The snapshots allow one to follow the evolutive process of growth, approximation, pairing and merging of two consecutive vortical structures in the axisymmetric jet shear layer region. As the snapshots show, owing to the exponential growth of the first vortice in the jet shear layer, the consecutive second vortice is rapidly accelerated, immediatly approximating, pairing and merging with the first at the end of jet potential core [Soh, 1994, Mitchell et al., 1999b, Bogey et al., 2003a]. The merging process of the two consecutive vortices generates a larger vortical structure, which is convected downstream by the flow in the near-field mixing region. The aerodynamic development of the vortical structures in the jet shear layer described above is in agreement with results obtained from simulations of axisymmetric round jets [Bogey, 2000] at the same flow conditions.

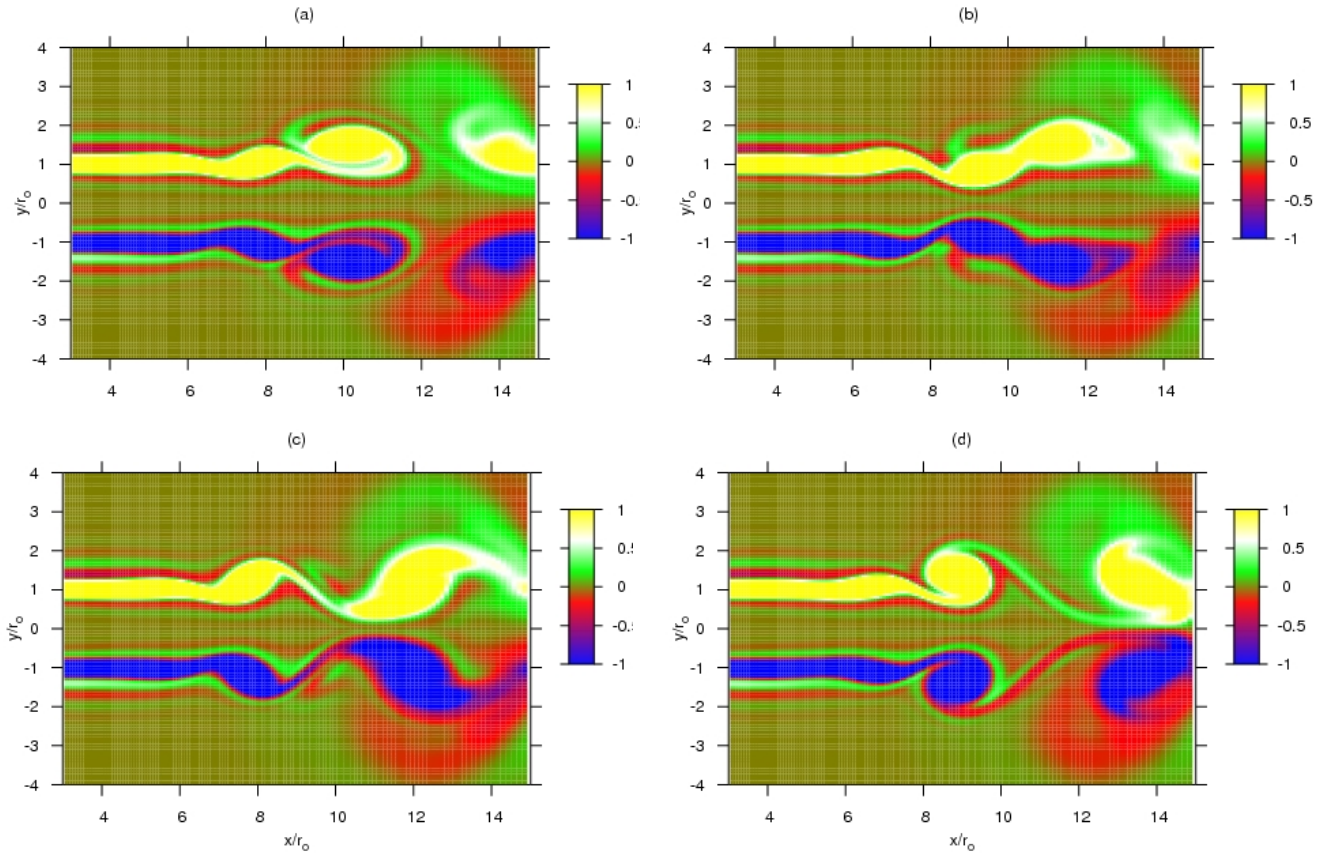

Figure 3. Aerodynamic development of the vortex pairing process on the round jet represented by the vorticity field ω_{xy} at four instants of time separated by $T_p/4$. Mixing region of the physical domain for $2 < x/r_o < 15$ and $-4 < y/r_o < 4$.

3.2 Acoustic field

The acoustic field corresponding to the vortex pairing process in the jet shear layer region described above is represented in Fig. 4 by the dilatation Θ at four sucessive instants of time separated by $T_p/4$. The acoustic field solution is displayed on the whole computational domain for $0 < x/r_o < 50$ and $-25 < y/r_o < 25$, except on the buffer zone of aerodynamic dissipation, located after $x/r_o = 15$ and for $-4 < y/r_o < 4$. Even with a relatively small width compared to the domain width, the buffer zone is able to efficiently dissipate all aerodynamic instabilities which arise in the near-field mixing region downstream of the vortex pairing location, avoiding the eventual appearance of other secondary

vortex pairing sound sources, which can contaminate the original acoustic field solution. It is important to remark that the fully computational domain is represented in Fig. 4. This domain does not require any artificial acoustic absorbing region at the outlow and at the far-field boundaries, what considerably simplifies the numerical implementation and reduces the computational cost.

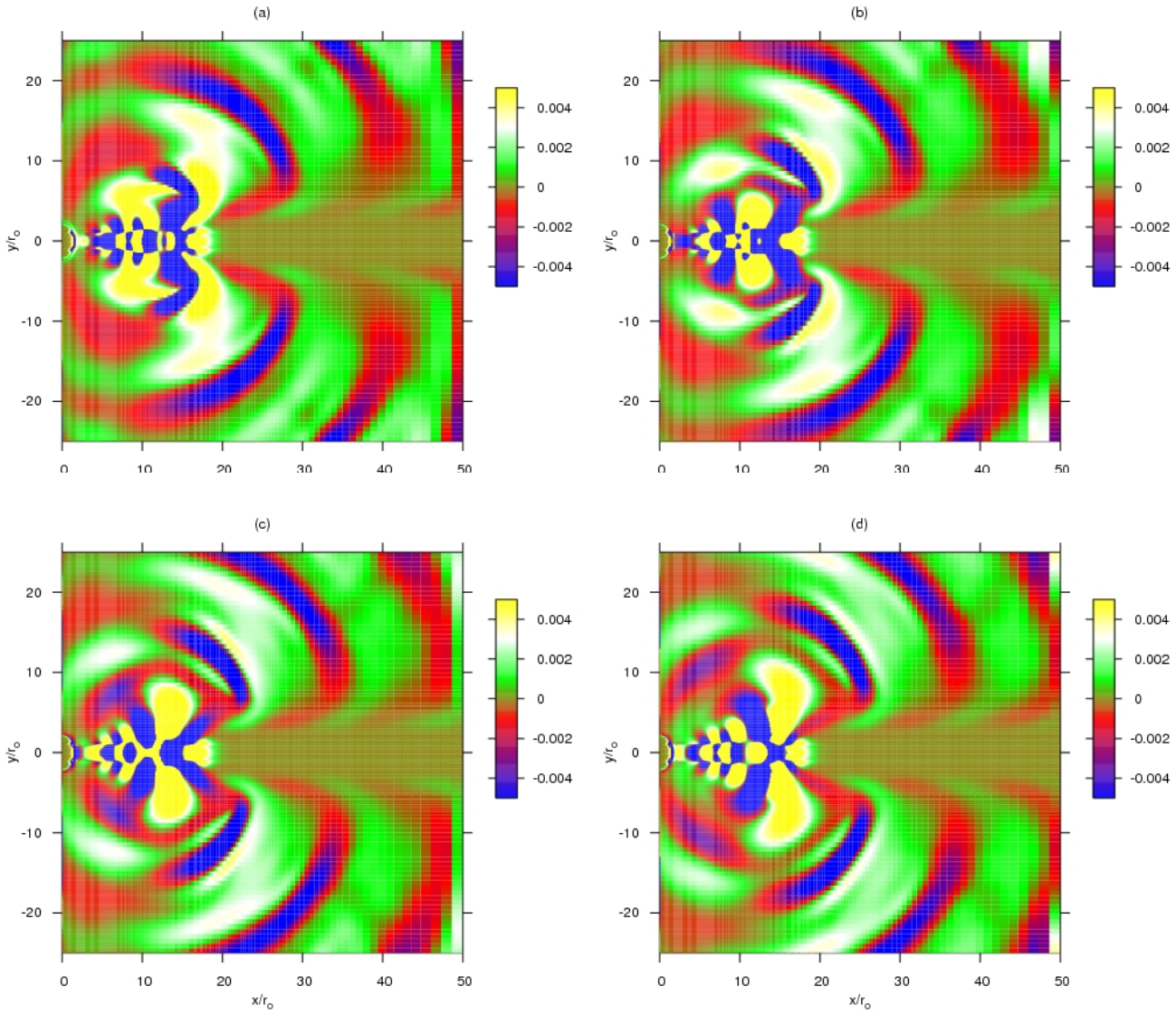

Figure 4. Acoustic field propagation from the round jet represented by the dilatation field Θ at four instants of time separated by $T_p/4$. The computational domain includes a buffer zone located after $x/r_o = 15$ and for $-4 < y/r_o < 4$.

3.3 Upper regions of aerodynamic and acoustic fields

In Figure 5 are displayed the upper regions of the aerodynamic and acoustic fields represented by the vorticity and dilatation, respectively. It is important to remark that both fields were directly computed by the implicit LES, without the need of any modeling approach. It should be noted in Fig. 5 that the acoustic wavefronts propagate from the shear layer region where occurs the vortex pairing process, which is located at the end of the potential core at around $x/r_o = 10$. Therefore, it was verified that the only dominant sound source produced in the jet shear layer is the sound radiated from the vortex pairing process, without any significant spurious wave oscillations provided by the near-inflow excitation region. This is due to its incompressible nature. It should be noted also that the acoustic waves propagate through the far-field boundary without producing any significant spurious wave reflections, because of the application of the non-reflecting boundary condition. The sound radiated by the vortex pairing process on the acoustic field decays to zero for an angle around 80^o, with phase shifting for wider angles of radiation relative to the jet shear layer axis. This particularly high directive character of sound radiation, especially noticed at high Mach numbers, is attributed to the axisymmetric

quadrupolar nature of the sound source, as already observed by LES of tridimensional jets [Bogey et al., 2003a].

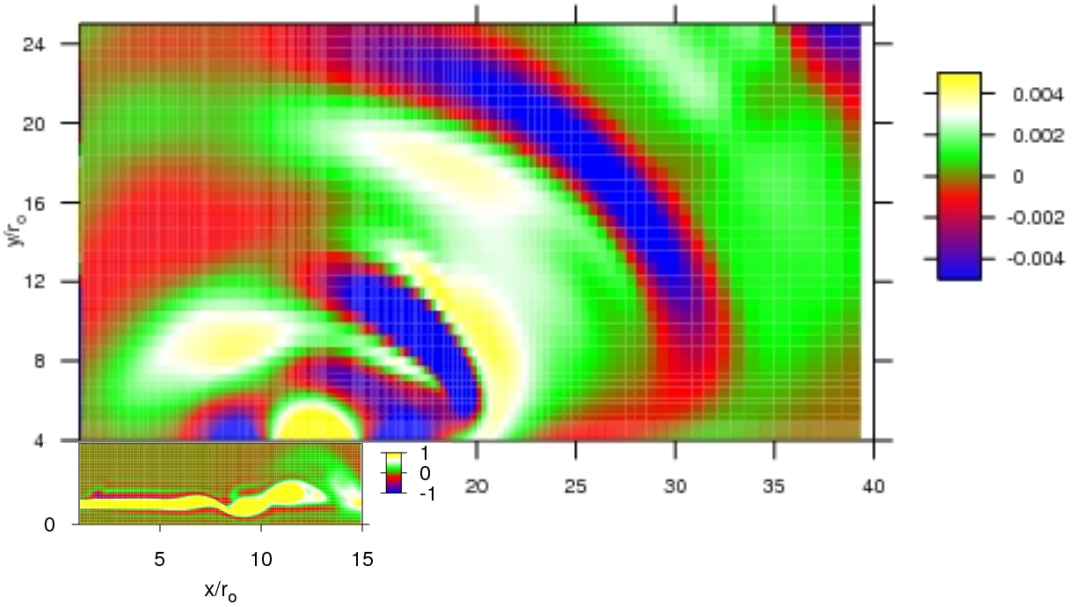

Figure 5. Upper regions of the aerodynamic and acoustic fields represented, respectively, by the dilatation Θ and vorticity ω_{xy} in a physical domain, excluding the buffer zone of aerodynamic dissipation located in the shear layer after $x/r_o = 15$.

4. CONCLUDING REMARKS

Mach number effects on sound radiation were investigated on a subsonic axisymmetric round jet at high Reynolds number. The preliminary results of noise radiation from a Mach 0.9 cold jet at Reynolds number 6.5×10^4 presented qualitative agreement with previous results taken from the literature at the same flow conditions. It was shown by the analysis of the aerodynamic field that the introduction of a periodic near-inflow excitation trigger the growth of shear layer instabilities, which rapidly evolve downstream to give rise to the vortex pairing process. By the analysis of the corresponding acoustic field propagation, it was verified that the only dominant sound source produced in the jet shear layer was the sound radiated from the vortex pairing process, without any significant spurious wave oscillations provided by the excitation. Due to its incompressible nature. The particularly high directive character of sound radiation, especially noticed at high Mach numbers, was attributed to the axisymmetric quadrupolar nature of the sound source.

In the ongoing works, thermal instability effects arising from the heated jet flow-noise sources intend to be investigated, as the presence of counter-rotating vorticity shear layers, already observed by direct numerical simulatations of non-isothermal mixing layers. It is hoped that high Reynolds number computations of both cold and heated jet flow-noise sources and its inherently coupled sound propagation will allow us to investigate more deeply the underlying nonlinear mechanisms by which noise is aerodynamically generated in turbulent shear layer flows at more real flow conditions.

5. ACKNOWLEDGEMENTS

This research project in computational aeroacoustics was supported by the LAE (Laboratory of Aerodynamics), Department of Aeronautical Engineering, University of São Paulo, Brazil. The project was sponsered by FAPESP (Fundação de Amparo à Pesquisa do Estado de São Paulo) which we gratefully thank for the financial support.

6. REFERENCES

D.J. Bodony and S.K. Lele. On using large-eddy simulation for the prediction of noise from cold and heated turbulent jets. *Phys. Fluids*, 17:85–103, 2005.

B. J. Boersma and S. K. Lele. Large eddy simulation of Mach 0.9 compressible jet. *AIAA paper 99-1874*, 1999.

C. Bogey. *Calcul direct du Bruit Aérodynamique et Validation de Modèles Acoustiques Hybrides*. PhD thesis, Ecole Centrale de Lyon, 2000.

C. Bogey and C. Bailly. Effects of inflow conditions and forcing on subsonic jet flows and noise. AIAA J. 43:1000-7, 2005a.

C. Bogey and C. Bailly. In *LES of a high Reynolds, high subsonic jet : effects of the subgrid modellings on flow and noise*, AIAA, Paper No. 2003-3557, 2003c.

C. Bogey and C. Bailly. Computation of a high reynolds number jet and its radiated noise using large eddy simulation based on explicit filtering. *Comput. Fluids*, 33:1344–1358, 2006.

C. Bogey and C. Bailly. In *Direct computation of the sound radiated by a high-Reynolds-number, subsonic round jet*, CEAS Workshop From CFD to CAA, 2002c.

C. Bogey and C. Bailly. In *LES of a high Reynolds, high subsonic jet : effects of the inflow conditions on flow and noise*, AIAA, Paper No. 2003-3170, 2003b.

C. Bogey, C. Bailly, and D Juvé. Noise investigation of a high subsonic, moderate Reynolds number jet using a compressible large eddy simulation. *Theor. Comput. Fluid Dyn.*, 16(4):273–297, 2003a.

D. Choi, T. J. Barber, and L. M Chiappetta. Large eddy simulation of High-Reynolds number jet flows. *AIAA paper 99-0230*, 1999.

T. Colonius, S. K. Lele, and P. Moin. Sound generation in a mixing layer. *J. Fluid Mech.*, 330:375–409, 1997.

N. El-Hady, T.A. Zang, and U. Piomelli. Application of the dynamic subgrid-scale model to axisymmetric transitional boundary layer at high speed. *Phys. Fluids*, 6:1299–1309, 1994.

G. Erlebacher, M.Y. Hussaini, C.G. Speziale, and T.A Zang. Toward the large-eddy simulation of compressible turbulent flows. *J. Fluid Mech.*, 238:155–185, 1992.

J. B. Freund, S. K. Lele, and P. Moin. Numerical simulation of a Mach 1.92 turbulent jet and its sound field. *AIAA Journal*, 38(11):2023–2031, 2000.

D. V. Gaitonde and M. R. Visbal. High-order schemes for Navier-Stokes equations: Algorithm and implementation into FDL3DI. *Technical Report AFRL-VA-WP-TR-1998-3060, Air Force Research Laboratory, Wright-Patterson, AFB*, 1998.

D. V. Gaitonde and M. R. Visbal. Further Development of a Navier-Stokes Solution Procedure Based on Higher-Order Formulas. *AIAA Paper No. 99-0557*, 1999.

D. V. Gaitonde, J. S. Shang, and J. L. Young. Practical aspects of high-order accurate finite-volume schemes for eletromagnetics. *AIAA Paper 97-0363*, 1997.

M. Germano, U. Piomelli, P. Moin, and W.H. Cabot. A dynamic subgrid-scale eddy viscosity model. *Phys. Fluids A*, 3: 1760–1765, 1991.

D. Juvé, M. Sunyach, and G. Compte-Bellot. Intermitency of the noise emission in subsonic cold jets. *J. Sound Vib.*, 71 (3):319–332, 1980.

J.C. Lau, P.J. Morris, and M.J. Fisher. Measurements in subsonic and suprsonic free jets using a laser velocimeter. *J. Fluid Mech.*, 1:1–27, 1993.

S. K. Lele. Compact finite difference schemes with spectral like resolution. *J. Comput. Phys.*, 103:16–42, 1992.

A. Leonard. Energy cascade in large eddy simulations of turbulent fluid flows. *Adv. Geophys*, 18A:237–248, 1974.

D. Lilly. A proposed modification of Germano subgrid-scale closure method. *Phys. Fluids*, 4:633–635, 1992.

P.A. Lush. Measurements of subsonic jet noise and comparison with theory. *J. Fluid Mech.*, 3:477–500, 1971.

A. Michalke. On the inviscid instability of the hyperbolic-tangent velocity profile. *J. Fluid Mech.*, 19:543–566, 1964.

Mitchell, B.E., Lele S., and P. Moin. Direct computation of the sound in an axisymmetric jet. *J. Fluid Mech.*, 383: 113–114, 1999a.

B. E. Mitchell, S. K. Lele, and P. Moin. Direct computation of the sound generated by vortex pairing in an axisymmetric jet. *J. Fluid Mech.*, 383:113–142, 1999b.

P. Moin, K.D. Squires, W.H. Cabot, and S. Lee. A dynamic subgrid-scale model for compressible turbulence and scalar transport. *Phys. Fluids A*, 3:2746–2757, 1991.

E. Mollo-Christensen, M.A. Kolpin, and J.R. Martucelli. Experiments on jet flows and jet noise far-field spectra and directivity patterns. *J. Fluid Mech.*, 18:285–301, 1964.

C. Moser, Lamballais, and Y. E. & Gervais. Direct computation of the sound generated by isothermal and non-isothermal mixing layers. *The 12th AIAA/CEAS Aeroacoustic conference, AIAA 2006-2447*, 2006.

N. Park, S. Lee, J. Lee, and H. Choi. A dynamic subgrid-scale eddy-viscosity model with a global model coefficient. *Phys. Fluids*, 18:125109, 2006.

A. Pascarelli, U. Piomelli, and G.V. Candler. Multi-block large-eddy simulations of turbulent boundary layers. *J. Comput. Phys.*, 257(256), 2000.

P. Sagaut. Large Eddy Simulation for Incompressible Flows. Springer Verlag, 2001.

W.Y. Soh. Unsteady flow computation towards noise predictions. 32nd Aerospace science meeting & Exhibit, Reno, NV, AIAA Paper 71-613, 1994.

C.G. Speziale, G. Erlebacher, T.A. Zang, and M.Y. Hussaini. The subgrid-scale modeling of compressible turbulence. *Phys. Fluids*, 31:940–942, 1988.

J.L. Stromberg, D.K. McLaughlin, and T.R. Troutt. Flow field and acoustic properties of a Mach number 0.9 jet at a low Reynolds number. *J. Sound Vib.*, 72(2):159–176, 1980.

H.K. Tanna. An experimental study of jet noise. Part I: Turbulent mixing noise. *J. Sound Vib.*, 50:405–428, 1977.

M. R. Visbal and D. V. Gaitonde. Very high-order spatially implicit schemes for computational acoustics on curvilinear meshes. *J. Comput. Acoust.*, 9(1):16–42, 2001.

M.R. Visbal and D.P. Rizzetta. Large-eddy simulation on curvilinear grids using compact differencing and filtering. *ASME: Journal of Fluids Engineering*, 124(4):836–847, 2002.

A. W. Vreman. An eddy-viscosity subgrid-scale model for turbulent shear flow: algebraic theory and applications. *Phys. Fluids A*, 16(10):3670–3681, 2004.

H. Yan and D. Knight. Large-eddy simulation of supersonic flat plate boundary layer part I. *AIAA Paper 2002-0132*, 2002.

K.B.M.Q. Zaman. Far-field noise of a subsonic jet under controlled excitation. *J. Fluid Mech.*, 152:83–111, 1985.

7. Responsibility notice

The authors are the only responsible for the printed material included in this paper.